npg

ORIGINAL ARTICLE

Structural-relaxation-driven electron doping of amorphous oxide semiconductors by increasing the concentration of oxygen vacancies in shallow-donor states

Han-Wool Yeon[1], Seung-Min Lim[1], Jung-Kyu Jung[1], Hyobin Yoo[1], Young-Joo Lee[1], Ho-Young Kang[1], Yong-Jin Park[1], Miyoung Kim[1] and Young-Chang Joo[1,2]

The electronic states of oxygen vacancies (V_O s) in amorphous oxide semiconductors are shallow donors, deep donors or electron traps; these are determined by the local atomic structure. Because the amorphous phase is metastable compared with the crystalline phase, the degree of structural disorder is likely to decrease, which is referred to as structural relaxation (SR). Thus SR can affect the V_O electronic state by changing the local atomic conditions. In this study, we demonstrated that electron doping is possible through the SR of amorphous oxides without redox reactions using a novel device structure that prevents extrinsic reactions with electrodes and ambient atmosphere during annealing. The concentration of V_O s in the shallow-donor state in amorphous In-Ga-Zn-O (a-IGZO) increases from $\sim 10^{16}$ to $\sim 10^{19}$ cm^{-3} with increasing annealing temperatures between 300 and 450 °C. The SR-driven doping effect is strongly dependent on the annealing temperature but not on the annealing time. The Arrhenius activation energy of the SR-driven doping effect is 1.76 eV, which is similar to the bonding energies in a-IGZO. Our findings suggest that the free volume in a-IGZO decreases during SR, and the V_O s in either deep-donor or electron-trap states are consequently transformed into shallow-donor states.

INTRODUCTION

Amorphous metal oxides, such as amorphous indium gallium zinc oxide (a-IGZO), have become mainstream materials for large-area and flexible electronics because the long-range structural disorder enhances the uniformity of the electrical properties and mechanical flexibility compared with crystalline metal oxides.[1–5] A notable characteristic of amorphous oxides, relative to their crystalline counterparts, is that these materials contain structural disorder-related defects (for example, free volume) in addition to non-stoichiometric defects (for example, oxygen vacancies), which significantly affect the corresponding electrical properties.[3,6–8] Moreover, the degree of structural disorder in amorphous metal oxides is always likely to decrease to form more stable structures because internal atomic rearrangement occurs even below the glass transition temperature (T_g). This process is known as structural relaxation (SR)[9–11] and results in continuous changes in the electrical properties. Thus understanding the effects of SR on the electrical properties of amorphous oxides is important for applications in future electronics.

In addition to uniformity and flexibility, amorphous metal oxides exhibit tunable electrical conductivity through redox reaction control

even after film formation.[12,13] These results indicate that oxygen vacancies (V_O s), which are inherent chemical defects, act as the dominant electron donors. Interestingly, the V_O s can act as deep donors[8] (that is, limited donation of free electrons), electron traps[3,6] and shallow donors, whose electronic states are determined by the local atomic environment. Certain researchers have suggested that all V_O s in crystalline IGZO are deep donors; however, certain V_O s act as shallow donors in a-IGZO when the structural disorder causes weak interactions between the metal ions and V_O s (that is, when the bonding distance between a metal ion and a V_O increases, called outward relaxation).[8] Other researchers have suggested that V_O s surrounded by large free volumes act as electron traps, whereas the shallow-donor state is formed when a V_O is located in a dense network.[3,6] In other words, disagreement exists with regard to which structural conditions are responsible for the V_O electronic states. However, the free electron concentration (n_e) in a-IGZO is thought to be affected by the degree of structural disorder in the amorphous phase because the electronic state of a V_O changes depending on the degree of structural disorder. Figure 1a presents a schematic illustration of the free volume changes in amorphous solids. T_f is the freezing

[1]Department of Materials Science and Engineering, Seoul National University, Seoul, South Korea and [2]Research Institute of Advanced Materials (RIAM), Seoul National University, Seoul, South Korea
Correspondence: Professor Y-C Joo, Department of Materials Science and Engineering, Seoul National University, 33-311, 1 Gwanak-ro, Gwanak-gu, Seoul 151-744, South Korea.
E-mail: ycjoo@snu.ac.kr
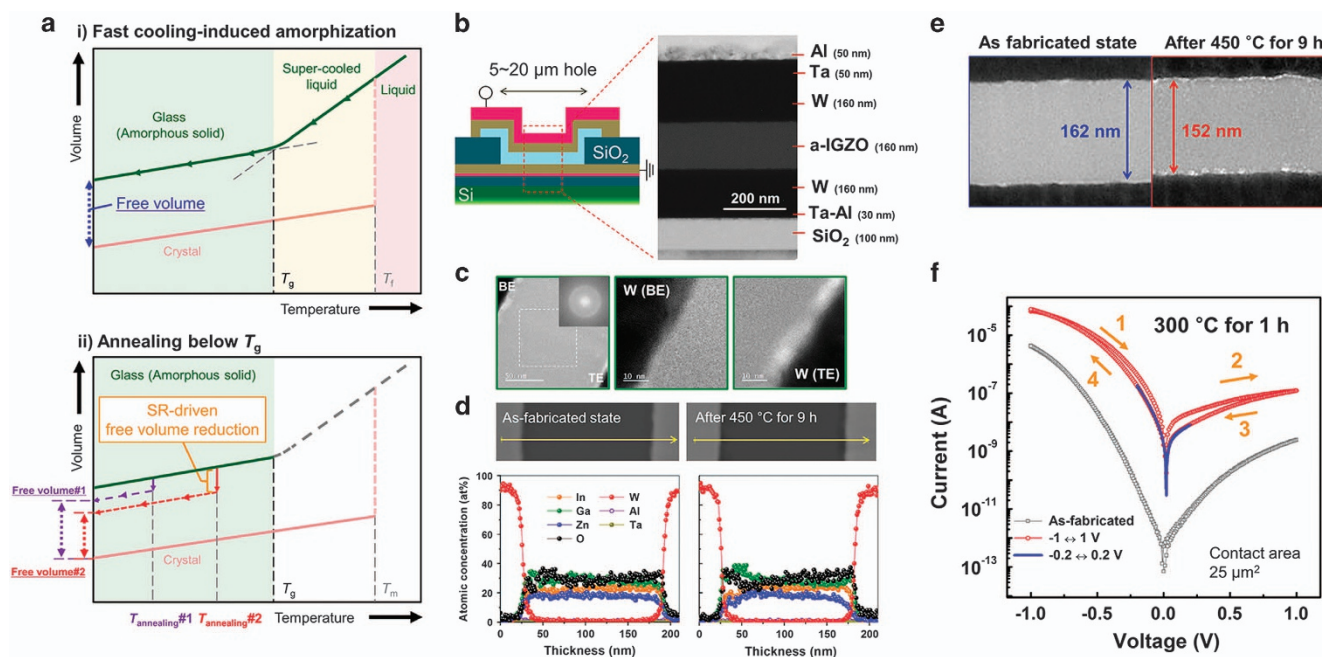
Figure 1 (**a**) Illustration of the free volume changes in amorphous solid during isothermal annealing below T_g. (**b**) Schematic structure of the devices used in this work. This structure prevents extrinsic reactions. A cross-sectional TEM image of the devices in the as-fabricated state is also shown. (**c**) High-resolution TEM images and fast Fourier transform (FFT) diffractograms of the devices after annealing at 450 °C for 9 h. The FFT analysis area is marked by the white-dotted line. (**d**) Magnified high-angle annular dark-field scanning TEM images (top) and energy dispersive X-ray spectroscopy (EDS) composition profiles of the devices along the arrow in the TEM images (bottom). (**e**) Thickness changes in a-IGZO thin-film patches after annealing at 450 °C for 9 h. A reduction in thickness of 6.2% was observed. (**f**) Representative current–voltage (*I*–*V*) characteristics of the devices in the as-fabricated state and after annealing at 300 °C for 1 h (measured at RT). In the as-fabricated state, rectifying *I*–*V* curves are observed even though the devices have a symmetric structure. After annealing at 300 °C for 1 h, counter figure-eight hysteretic *I*–*V* curves are observed in the voltage range from − 1 to 1 V.

temperature and T_m is the melting temperature. The difference in the solid volume between the amorphous phase and the crystalline state represents the free volume in the amorphous solid.[14] When amorphous solids are annealed below T_g, SR occurs and the free volume decreases because internal atomic rearrangement occurs without significant long-range migration.[9–11] Thus SR can induce changes in n_e in a-IGZO through changes in the electronic states of the V_O s. Therefore, understanding the effects of SR on the concentration of V_O s in the shallow-donor state (N_{DS}) and n_e in a-IGZO is important for developing device-level a-IGZO applications and reliable resistance to thermal stress. However, only a few studies, if any, exist on the SR effect on either N_{DS} or n_e in a-IGZO.[15–19] Although there have been reports on the effects of postdepositional annealing on the electrical properties of a-IGZO thin films, our understanding of the SR effect remains insufficient because the interactions with the atmosphere[15–18] and/or metal electrodes[19] during annealing also affect the electrical properties of a-IGZO. Therefore, the interaction of a-IGZO with the ambient atmosphere and metal electrodes during thermal annealing should be prevented to ensure that only the SR effect is responsible for changes in the electrical properties of a-IGZO.

Here we investigate the changes in the electronic states of V_O s in a-IGZO owing to SR without ambient artifacts by using vertically structured novel metal/a-IGZO/metal devices. The metal electrodes are composed of tungsten (W) and a tantalum (Ta)–aluminum (Al) multilayer, which act as the non-reactive electrode and gastight layers, respectively. The interaction with the ambient atmospheres and the interfacial reaction with electrode materials were effectively prevented by covering the a-IGZO dot patterns with the metal electrodes. After the devices were fabricated, annealing was performed in the

temperature range of 300–450 °C, that is, below T_g[11] for 1 to 16 h. After postfabrication annealing, the changes in the direct current (DC) current–voltage (*I*–*V*) characteristics of the devices were measured with respect to the substrate temperature. Based on the annealing conditions, the devices exhibited different conduction mechanisms, that is, Schottky thermionic, Ohmic and Poole–Frenkel conduction (P-F).

In this study, we quantified the SR-driven doping effect by analyzing the conduction mechanisms of the devices after exposure to the various annealing conditions. The N_{DS} and n_e in the a-IGZO increased in the devices with increasing annealing temperature. After annealing at 300 °C, the value of N_{DS} was on the order of 10^{16} cm^{-3}. With increasing annealing temperature up to 450 °C, N_{DS} increased $>10^3$ times. Despite the lack of changes observed in the absolute V_O concentration, these results suggest that changes occurred in the n_e in a-IGZO because V_O s at the deep-donor or electron-trap level were transformed into the shallow-donor state owing to SR. To the best of our knowledge, we are the first to report that structural changes in amorphous metal oxide semiconductors significantly alter N_{DS} and n_e.

MATERIALS AND METHODS

A 30-nm-thick Ta-Al bilayer was deposited on a SiO₂ (100 nm)/Si wafer using DC sputtering as the adhesive layer. For the bottom electrode (BE) of the devices, 160-nm-thick W was deposited on the Ta-Al adhesive layer. A 500-nm-thick SiO₂ isolation layer was deposited by plasma-enhanced chemical vapor deposition at a substrate temperature of 300 °C. Throughgoing holes were patterned in the isolation layer using photolithography and dry etching, and the area was varied from 25 to 400 µm². This step was followed by radiofrequency (RF) sputtering of 160-nm-thick a-IGZO, using a polycrystalline InGaZnO₄

target at room temperature (RT). The key process conditions were as follows: 50-W RF power under working pressure of 5 mTorr, and argon (Ar) and O_2 process gas flow rates of 19 and 1 sccm (that is, an O partial pressure of 3.3×10^{-2} Pa), respectively. Investigation of the stoichiometry, structural properties and optical properties of as-deposited a-IGZO thin films is important because the SR phenomena would be dependent on the initial characteristics of the films.[15,20–22] The chemical composition of the deposited a-IGZO films was In:Ga:Zn = 1:1.6:0.8 (atomic ratio), as revealed by X-ray photoelectron spectroscopy (Supplementary Figure S1). The film density and optical band gap of the films are 5.8 g cm^{-3} and 3.14 eV, respectively, which are similar to those of previous reports[6,23] (details of the measurement are provided in Supplementary Figure S2). Moreover, tail-like optical absorptions are observed beneath the band gap (Supplementary Figure S2d). This confirms that subgap states (for example, deep-donor states near the valence band maximum, continuous trap level) initially existed in a-IGZO.[6,15,20] Using photolithography followed by dilute HF etching, the a-IGZO thin films were patterned into square-shaped patches; the area of each patch was 6400 μm^2 to fill the SiO_2 hole. The top electrode (TE) consisted of a W (160-nm thick)/Ta-Al (100-nm thick) stack that was DC-sputtered in a blanket layer and patterned using the lift-off process to cover the a-IGZO patches. The Ta-Al bilayer blocks were inserted between the a-IGZO and the ambient atmosphere. The resultant devices were annealed at temperatures between 300 and 450 °C for up to 16 h under vacuum (10^{-3} Pa). For the annealing process, the temperature increased at a heating rate of 5 °C min^{-1} from RT to the target annealing temperature, followed by maintenance of the target temperature for the specified duration. After annealing, the I–V characteristics of the devices were measured using an 4156C parameter analyzer (Agilent Technologies, Santa Clara, CA, USA). Voltage was applied to the TE, whereas the BE was grounded. The substrate temperature was varied from RT to 96 °C. At each annealing condition, 10–50 devices were considered to evaluate the changes in the electrical properties of a-IGZO. Cross-sectional images of the as-fabricated devices and after annealing at 450 °C for 9 h were collected using a transmission electron microscope (TEM; JEOL, Tokyo, Japan, JEM-2100F). The TEM samples were fabricated using a focused ion beam (SMI3050SE, SII NanoTechnology, Chiba, Japan). Scanning TEM-EDS (energy dispersive X-ray spectroscopy) composition profiles of the devices were also obtained. An X-ray photoelectron spectroscopy (PHI-5000 Versa Probe, Phi Physical Electronics, Chanhassen, MN, USA) was used to measure the changes in the compositions and chemical states of the elements in the Ta-Al/W/a-IGZO/W/Ta-Al films that have the same dimension as the devices after annealing.

RESULTS AND DISCUSSION

Figure 1b schematically shows the vertical structure of the devices. We selected W as the non-reactive electrode material because it does not interact with nor diffuse into a-IGZO, its Gibbs free energy of oxide formation is higher than that of In_2O_3, Ga_2O_3 and ZnO[24] and its melting temperature is sufficiently high,[25] thereby minimizing thermal diffusion into a-IGZO. The Ta-Al films on the W TE prevent interfacial interaction between a-IGZO and the ambient atmosphere because the native oxide formed passivates the film surface.[26] The 160-nm-thick a-IGZO patches are covered with a TE consisting of the non-reacting W and the Ta-Al bilayer; thus extrinsic reactions in addition to SR are prevented during postfabrication annealing as demonstrated in Figures 1c–e and Supplementary Figures S1. Under the most severe thermal stressing conditions in our experiments, that is, annealing at 450 °C for 9 h, interface reactions, crystallization and interdiffusion did not occur in the a-IGZO, which was confirmed using TEM analysis (Figures 1c and d). Interestingly, the a-IGZO film thickness was reduced by 6.2% after annealing at 450 °C for 9 h (Figure 1e). These results directly show that the reduction in free volume in a-IGZO was due to SR (further details of TEM analysis results are provided in Supplementary Figure S3). Moreover, changes in the chemical states of In, Ga, Zn, O (or V_O) and W in the a-IGZO were not detected by X-ray photoelectron spectroscopy

(Supplementary Figure S1). When the Ta-Al bilayer was not covered with the TE, the I–V characteristics after annealing were affected by the ambient atmosphere (Supplementary Figure S4). The electrical conductance of the devices without Ta-Al under reducing ambient conditions are higher than those of the devices under oxidizing ambient conditions. However, the changes in the I–V characteristics of the devices with Ta-Al appear negligible after annealing in ambient atmosphere. These results strongly suggest that the fabricated devices effectively inhibit extrinsic reactions in the a-IGZO and maintain the absolute V_O concentration in a-IGZO during annealing.

Figure 1f presents the semi-logarithmic I–V curves of the devices in the as-fabricated state and those of the devices after annealing at 300 °C for 1 h, all of which were measured at RT. Rectifying behavior is observed in the as-fabricated devices. This behavior indicates that the electrical conduction of the devices is limited by the Schottky barrier at the W/a-IGZO contact. Ideally, a Schottky barrier is formed at the a-IGZO/W interface because the electron affinity of a-IGZO[27] is lower than the work function of W[28] (the corresponding energy band diagram is provided in Supplementary Figure S5a). When a negative bias is applied to the TE, the electrical conductance is much higher than that under positive bias conditions, indicating that, although the devices have a symmetric structure, an effective Schottky barrier is formed at the a-IGZO/BE interface rather than at the TE/a-IGZO interface. The lower barrier height at the TE interface than that at the BE interface may be due to the generation of interface states (for example, O-deficiency-related defects and metal-induced gap states) during TE deposition.[29] Therefore, the dominant conduction mechanism of the devices as fabricated is attributed to the Schottky barrier at the BE interface.

After annealing at 300 °C for 1 h, the asymmetric I–V curves were maintained; however, the electrical conductance of the devices increased relative to the as-fabricated state. This finding indicates that the conduction of the devices was still dominated by the Schottky barrier at the BE interface but that the barrier height decreased after the annealing.[29–31] The Schottky barrier height decreased because the N_{DS} in the a-IGZO increases after annealing; thus the net positive charges in the depletion region increased.[29–32] Because changes in the concentration of O (or V_O s) in the a-IGZO is prohibited in the devices during annealing, we suggest that neutral V_O s in the deep-donor state in the a-IGZO are transformed into a positively charged shallow-donor state, increasing the N_{DS}.

A remarkable counter figure-eight hysteretic I–V loop is observed in the voltage range from −1 to 1 V after annealing. This characteristic I–V hysteresis shape indicates that the Schottky barrier height or width at the BE interface is modulated with respect to the bias polarity in association with electron trapping/detrapping in the vicinity of the BE interface.[31] Under a negative bias, electron detrapping occurs, and the net positive charge in the depletion region increases, causing a decrease in the height or width of the Schottky barrier and increased electrical conductance. However, when a positive bias is applied, positively charged electron-trap states become neutral as electrons are captured, increasing the height or width of the Schottky barrier. This result indicates that electron-trap sites as well as V_O s in the shallow-donor state dominate the positively charged depletion region. Because the hysteresis disappeared in the voltage range of −0.2 to 0.2 V, the degree of the Schottky barrier height/width modulation was dependent on the magnitude of the current. In the as-fabricated state, as the voltage sweep range increased, more current was produced in the devices, and the I–V curves also exhibited counter figure-eight hysteretic behavior as shown in Supplementary Figure S6. This finding suggests that a sufficient number of V_O s act as electron traps in the

4
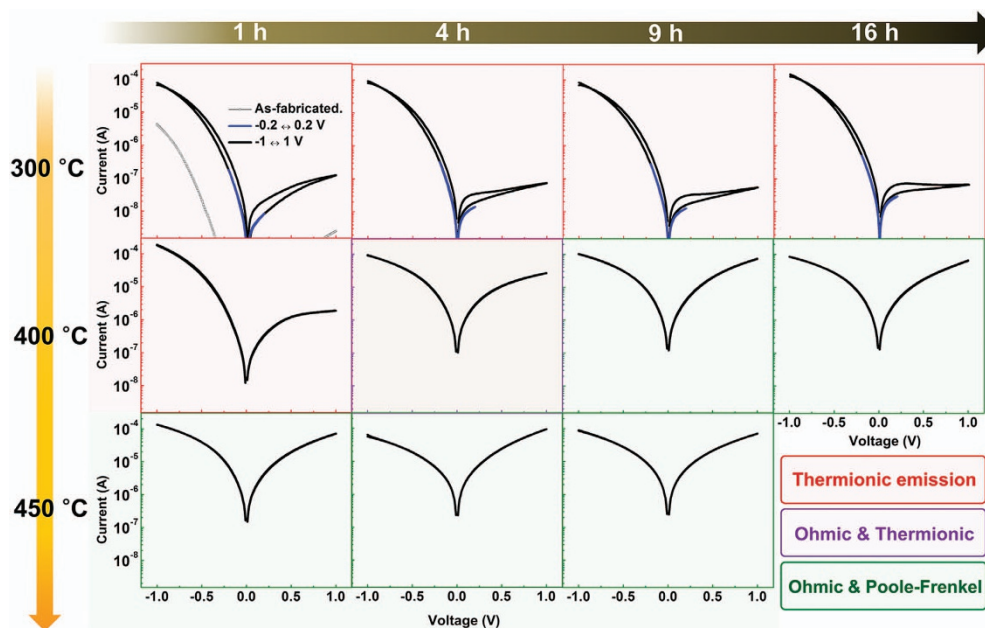
Figure 2 I–V map of the devices considering both annealing temperatures from 300 to 450 °C and annealing times from 1 to 16 h. The contact area of the devices was 25 μm². After annealing at 300 °C, the rectifying and hysteretic behaviors with similar electrical conductance are observed even after the annealing time of 16 h. After annealing at 400 °C, the hysteresis disappears with an increase in the electrical conductance, and the I–V curves become symmetric as the annealing time increases. When the I–V curves become symmetric, the I–V characteristics are nearly constant regardless of further annealing. After annealing at 450 °C, symmetric I–V curves are observed even after an annealing time of 1 h.

a-IGZO to affect electrical conduction in both the as-fabricated devices and the devices annealed at 300 °C for 1 h.

Figure 2 presents a map of the I–V curves of the devices with respect to the postfabrication annealing conditions, in which the temperature was varied from 300 °C to 450 °C for 1–16 h. At 300 °C, the rectifying and hysteretic I–V characteristics and similar electrical conductance are observed even after an annealing time of 16 h. As the annealing temperature increases to 400 °C, the electrical conductance of the devices increases more than at 300 °C. Moreover, the hysteresis of the I–V curves disappeared after annealing for 1 h. These results suggest that, as the annealing temperature increases to 400 °C, the N_{DS} increases, whereas the concentration of V_O s that act as electron traps becomes negligible with respect to the V_O s in the shallow-donor state. Previous studies report that extra subgap states located ~ 0.2 eV below the conduction band minimum (E_C) induce hysteretic I–V behavior in as-fabricated a-IGZO thin-film transistors.[16] Moreover, the postannealing process annihilates the subgap states, resulting in an enhancement of the electrical performance of the thin-film transistors, including the disappearance of the hystereis.[16] Therefore, we believe that the V_O s in the electron-trap states are the origin of the extra subgap states in a-IGZO and are annihilated during postfabrication annealing through SR.

At an annealing temperature of 400 °C, the asymmetry of the I–V curves decreases with longer annealing time. Symmetric I–V curves appeared after an annealing duration longer than 9 h, beyond which the I–V characteristics changed little up to 16 h. At 450 °C, symmetric I–V curves were observed after annealing for only 1 h, and the electrical conductance increased even further. These I–V characteristics were maintained up to an annealing time of 9 h. The I–V characteristics can be summarized as follows. The electrical conductance of the devices increases at higher annealing temperatures. Symmetric I–V curves appeared with annealing temperature higher than 400 °C. The changes in the electrical properties of a-IGZO due to SR appear to be

determined by the annealing temperature rather than the annealing time; the annealing time-independent behavior is another piece of evidence that time-dependent extrinsic reactions (for example, diffusion of impurities, redox reactions) did not occur during annealing.

At an annealing temperature of 300 °C, the dominant conduction mechanism of the devices is related to overcoming the Schottky barrier at the BE interface as noted above. The carrier transport mechanisms at the Schottky contact are attributed to both thermionic emission and field emission (that is, tunneling), and the contribution of the latter increases with higher carrier concentration in the semiconductors and/ or defect density at the Schottky contact.[29] When field emission is the dominant conduction mechanism, the current in the reverse bias regime exhibits exponential behavior as a function of the applied voltage, whereas a weak-voltage-dependent reverse current is observed under thermionic emission.[29,32] Because the devices annealed at 300 °C indicate that the reverse current is weakly dependent on the applied voltage, thermionic emission dominates the conduction mechanism. Because the n_e in the a-IGZO thin-film patches in as-fabricated devices is $< 10^{16}$ cm^{-3} (Supplementary Figure S7), thermionic emission is the dominant conduction mechanism at the Schottky contact at the a-IGZO/BE interface.[29] Supplementary Information can be consulted for further description of this increased contribution of field emission to the carrier transport in terms of the increased initial n_e (or N_{DS}) in a-IGZO thin-film patches in the as-fabricated devices.

Figure 3a shows the change in the Schottky diode parameters, including the Schottky barrier height (Φ_B) and ideality factor (n) of the devices after annealing based on thermionic theory under forward bias conditions.[30] After annealing at 300 °C, the Φ_B decreased with increasing n compared with that in the as-fabricated state, implying increased contribution of the field emission to the Schottky conduction.[29] Therefore, certain V_O s at the deep-donor level are transformed into shallow donors and/or electron traps after annealing,
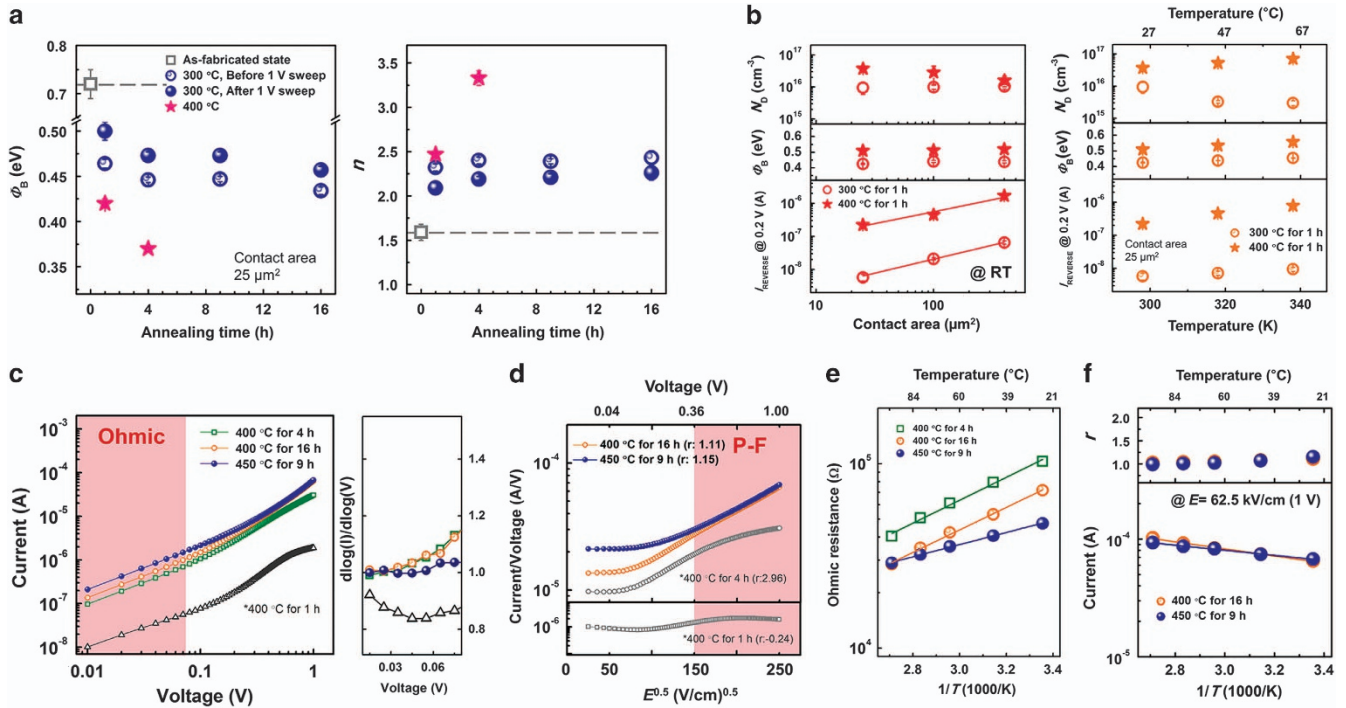
Figure 3 Conduction mechanism analysis of the devices after annealing. (a) The variations in the Schottky diode parameters in the devices after annealing at 300–400 °C: Schottky barrier (Φ_B) and ideality factor (n) at RT. The contact area of the devices was 25 μm^2. (b) Dependence of the reverse current ($I_{REVERSE}$), Φ_B and the concentration of positively charged defects in the depletion region of a-IGZO (N_D) on the contact area and temperature. (c) Double-logarithmic I–V plots and the slope of the corresponding plots to determine the Ohmic conduction. (d) Log(I/V)-$E^{0.5}$. plots to identify the P-F conduction. Arrhenius plots of (e) Ohmic resistance and (f) the current at $E = 62.5$ kV cm^{-1} with the P-F parameter r.

and the n_e in a-IGZO and/or the defect density in the vicinity of the BE interface increases. This finding is consistent with the explanation of the origin of the increased electrical conductance in the annealed devices relative to that of the as-fabricated devices. Furthermore, decreases in the series resistance (R_S) of the devices after being annealed at 300 °C (Supplementary Figure S8) may indicate that the n_e in a-IGZO increases relative to the as-fabricated state owing to annealing-related SR.

The variation in Φ_B based on the applied voltage history appears to agree with the origin of the counter figure-eight I–V curve. The V_O s in the electron-trap state significantly affect the net positive charges in the depletion layer in the vicinity of the a-IGZO/BE interface. The increase in Φ_B and the decrease in n associated with the application of a positive bias demonstrates that the net positive charges in the depletion region decrease as electron trapping occurs. Based on such characteristic changes in the Schottky parameters, we would expect Φ_B to decrease and n to increase with further annealing time. However, the corresponding kinetics becomes dramatically retarded after an annealing time of 1 h. Therefore, the SR effects on the electrical properties of a-IGZO are primarily related to the annealing temperature rather than the annealing time.

To quantify N_{DS} in the a-IGZO after annealing at 300 °C, the I–V characteristics under reverse bias conditions have been considered. When the applied voltage is higher than the value of $3k_BT/q$, the reverse current ($I_{REVERSE}$) is given by[33]:

$$I_{REVERSE} = I_S \exp\left(\frac{0.34q(q/\varepsilon_{IGZO}\varepsilon_0)^{3/4}N_D^{1/4}(V + V_{bi} - k_BT/q)^{1/4}}{k_BT}\right),$$

(1)

where k_B is Boltzmann's constant, q the electron charge, T the absolute temperature, I_S the saturation current, ε_{IGZO} the relative dielectric constant (10 for a-IGZO[27]), ε_0 the permittivity of vacuum, V_{bi} the built-in potential and N_D the concentration of the positively charged defects in the depletion region. The parameter V_{bi} is expressed as[33]:

$$V_{bi} = \frac{1}{q}\left[\Phi_B + k_BT\ln\left(\frac{N_D}{N_C}\right)\right],$$

(2)

where N_C is the effective density of the conduction band states (5×10^{18} cm^{-3} for a-IGZO[27]). The saturation current, I_S, is given as[33]:

$$I_S = AA^*T^2\exp\left(-\frac{\Phi_B}{k_BT}\right),$$

(3)

where A is the contact area, A^* is the effective Richardson constant ($A^* = 40.8$ A cm^{-2} K^{-2} for a-IGZO[27]).

The value of N_D was extracted using Equations (1)–(3),, and the values of Φ_B and $I_{REVERSE}$ at 0.2 V ($> 3k_BT/q$) from the non-hysteretic I–V curves in the voltage range from -0.2 to 0.2 V. Figure 3b shows the dependence of $I_{REVERSE}$ at 0.2 V and Φ_B of the devices after annealing at 300 °C for 1 h on the contact area and substrate temperature. Although $I_{REVERSE}$ at 0.2 V increases with the contact area and the substrate temperature, the value of N_D remains relatively constant. Therefore, the dominant conduction mechanism of the devices corresponds to thermionic emission. Slight changes in N_D with respect to the contact area and substrate temperature may be induced such that the conduction mechanism of the devices deviated from ideal thermionic emission theory, the value of n is >1 and $I_{REVERSE}$ does not exhibit a linear relationship with the contact area (that is, the slope of the solid lines in Figure 3b are 0.85 and 0.72 for the devices after annealing at 300 °C for 1 h and at 400 °C for 1 h, respectively). After annealing at 300 °C for 1 h,

the N_D in the a-IGZO of the devices was determined to be 9.98 (±2.52)$\times10^{15}$ cm^{-3}. In addition to 1 h, the N_D for the a-IGZO following annealing at 300 °C for a range of annealing times up to 16 h is shown in Figure 4b. Similar to the I–V characteristics, N_D is nearly constant with further annealing, suggesting that the SR effect on the N_D in a-IGZO is not dependent on the annealing time. At the annealing temperature of 400 °C, thermionic emission is the dominant conduction mechanism up to an annealing time of 4 h. Compared with 300 °C, Φ_B decreased, whereas n increased (Figure 3a). These results suggest that higher N_D values are expected in a-IGZO at annealing temperatures of 400 °C.[29] The N_D in the a-IGZO after annealing at 400 °C for 1 h was determined to be 3.28 (±1.32)$\times10^{16}$ cm^{-3} (Figure 3b). Thus, as the annealing temperature increased from 300 to 400 °C, the N_D increased approximately three times owing to SR. Based on the observed hysteretic behavior, the extracted N_D value after annealing at 300 °C represents the summation of the N_{DS} and the concentration of V_O s in the electron-trap state. After annealing at 400 °C, however, the hysteresis disappears, and the N_D corresponds to N_{DS}. With increasing annealing time up to 4 h, Φ_B decreases and n increases (Figure 3a). Based on Equations (1)–(3), the N_{DS} value is calculated to be 9.43 (±4.77)$\times10^{16}$ cm^{-3} at RT (Supplementary Figures S9a and b). In addition to the analysis of the reverse current characteristics, investigation of the capacitance (C) characteristics in the Schottky diodes is an effective method for extracting N_D values and trap energy levels from semiconductors.[33,34] However, the devices in this study have a parasitic capacitance and poor Ohmic contacts at the TE/a-IGZO interface (Supplementary Figure S10). These factors interfere with the accurate estimation of the C characteristics in the Schottky diodes, resulting in

difficulty extracting the N_D (or trap energy level) in a-IGZO (details of C–V characteristics of the devices are introduced in Supplementary Figures S11–S13). Therefore, we believe that the precise reverse current analysis of the Schottky conducting devices is the best way to investigate the changes of N_D in a-IGZO due to SR.

The devices after annealing at 400 °C for 4 h exhibit Ohmic conduction in the low voltage region (<0.07 V) as shown in Figure 3c. The slope of the double-logarithmic I–V curve is close to 1, whereas the slopes of the devices after annealing at 400 °C for 1 h deviate from 1. Moreover, the devices that exhibit symmetrical I–V curves also follow Ohmic conduction in the low voltage region. As the applied voltage increased, the conduction mechanism transformed to non-Ohmic conduction. The symmetric I–V curve can be explained by the change in the Schottky contact resistance at the TE/a-IGZO interface to a value similar to that of the a-IGZO/BE interface or the transition of the predominate conduction mechanism to bulk-limited conduction. The candidates responsible for such non-Ohmic and bulk-limited conduction mechanisms in the devices are P-F conduction and space-charge-limited current.[33] Considering the magnitude of the applied electric fields in the a-IGZO thin-film patches and the temperature dependence of the electrical conductance (Figures 3e and f), the conduction mechanisms based on tunneling can be neglected.[33]

The P-F conduction is given as:[35,36]

$$I_{P-F} \propto E\exp\left[\frac{1}{rk_BT}\left(q\sqrt{\frac{qE}{\pi\varepsilon_{IGZO}\varepsilon_0}} - \Phi_{PF}\right)\right], \qquad (4)$$

where E is the applied electric field (approximately V divided by 160 nm), Φ_{PF} is the P-F barrier and r is a constant ranging from 1 to
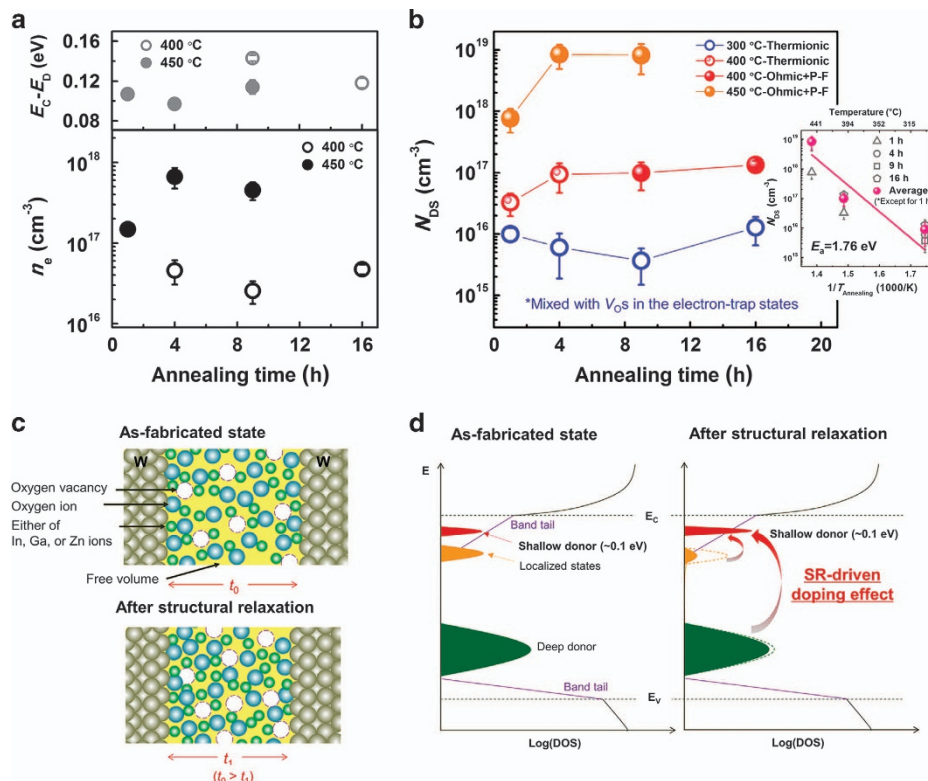
Figure 4 (**a**) The changes in the free electron concentration (n_e) and shallow-donor energy level ($E_C - E_D$) of V_Os in a-IGZO after annealing at 400 and 450 °C. (**b**) The V_O concentration in the shallow-donor state (N_{DS}) in a-IGZO with respect to postfabrication annealing conditions. The N_{DS} in a-IGZO after annealing at 300 °C includes the concentration of V_O in the electron-trap states. Illustrations of the (**c**) atomic rearrangement of a-IGZO in the devices and (**d**) the change in the density of states (DOS) in a-IGZO owing to SR. The DOS configuration in a-IGZO in the as-fabricated state was obtained from Kamiya et al.[3] and Ide et al.[43]

2. Figure 3d presents the $\log(I/V)$ vs $\sqrt{E}$ plot for the devices under positive bias conditions. The parameter r is derived from the slope of the $\log(I/V)$ vs $\sqrt{E}$ curve in the range from 22.5 to 62.5 kV cm^{-1}. The devices after annealing at 400 °C for 1 and 4 h are not well fitted by the orthodox P-F conduction theory. However, because r for the devices showing symmetric I–V curves varies between 1 and 2, P-F conduction is the dominant conduction mechanism for the devices that exhibit symmetric I–V curves in the high voltage region (0.36–1.0 V). Thus the conduction mechanism of the devices with symmetric I–V characteristics can be expressed as follows: (i) In the low-field region, thermally excited electrons from V_O s in the shallow-donor state primarily flow above the E_C. (ii) As the magnitude of E increases, the free electrons from V_O s in the shallow-donor state, assisted by the electric field and P-F conduction, become predominant. The I–V characteristics of the devices did not match the space-charge-limited current mechanism (Supplementary Figure S14). The conduction mechanism consists of Ohmic conduction in the low-field region and P-F conduction in the high-field region, which is analogous to reports on the conduction mechanisms of several amorphous materials, including a-IGZO.[36–38] Because the Φ_{PF} corresponds to $E_C - E_D$, where E_D is the location of the donor energy level,[36] the energy level of the V_O s at the shallow-donor states can be estimated from the temperature dependence of the P-F current.

Figure 3e shows the temperature dependence of the Ohmic resistance in the devices. As the annealing temperatures increase, the resistance decreases. The Arrhenius equation fits these values well. The temperature dependence of the Ohmic resistance is primarily affected by the change in n_e in a-IGZO.[30,33] The value of n_e is expressed as:[30]

$$n_e = N_C \exp\left(\frac{E_F - E_C}{k_B T}\right), \tag{5}$$

where E_F is the Fermi level. Thus the slope of the solid lines in Figure 3e represents $(E_F - E_C)/k_B$, and n_e in a-IGZO at RT can be estimated to be N_C as reported in Fung et al.[27] Figure 4a shows the value of n_e in a-IGZO after annealing at 400 and 450 °C, respectively. After annealing at 400 °C for 4 h, the values of n_e at RT is calculated to be 4.56 ($\pm$1.52) $\times 10^{16}$ cm^{-3} based on the results of the changes in the Ohmic resistance (Figure 3e). At an annealing time of 16 h, the value of n_e barely changes (4.72 ($\pm$0.65) $\times 10^{16}$ cm^{-3}). However, at the higher annealing temperature of 450 °C (for 9 h), the slope of the resistance changes decreases (Figure 3e), and the value of n_e increases to 4.53 ($\pm$1.14) $\times 10^{17}$ cm^{-3}. Therefore, with higher annealing temperatures, N_{DS} increases because V_O s in the deep-donor or electron-trap states are transformed into shallow donors owing to SR. Thus n_e is more strongly affected by the annealing temperature than the annealing time.

In addition to the Ohmic resistance, the P-F parameter r and the P-F current (at 1 V) are plotted with respect to the substrate temperature in Figure 3f. The constant value of r regardless of the temperature demonstrates that P-F conduction is the dominant conduction mechanism for the devices. The Φ_{PF} was extracted from the slope of the solid lines in Figure 3f. After annealing at 400 °C for 16 h, the Φ_{PF} was determined to be 0.12 ($\pm$0.01) eV, and Φ_{PF} exhibits a lower value of 0.11 ($\pm$0.01) eV after annealing at 450 °C for 9 h (Figure 4a). These extracted values are similar to those in the previous reports on the donor energy levels in a-IGZO (~0.11 eV).[39] Moreover, the shallower-donor energy levels associated with higher n_e values can be explained by the screening effect.[39,40] Therefore, the estimated value of the energy level of V_O s at the shallow-donor state through analysis of P-F conduction is highly reliable. Because the value of $E_C - E_D$ is

higher than the value of $k_B T$, the field-enhanced thermal excitation of free electrons (that is, P-F conduction) is possible.

Because the location of E_F and E_D are known, the value of N_{DS} in a-IGZO after annealing at 400–450 °C can be estimated as follows. The actual donation of free electrons from the shallow-donor states at a given substrate temperature is given by:[33]

$$n_e = N_{DS} \left[1 / \left(1 + 2\exp\left(\frac{E_F - E_D}{k_B T}\right) \right) \right]. \tag{6}$$

Based on the results in Figure 4a, N_{DS} in a-IGZO after annealing at 400–450 °C is extracted as shown in Figure 4b. The cumulative distribution of N_{DS} in a-IGZO (as well as the electrical parameters related to N_{DS}) is shown in Supplementary Figure S15. The value of N_{DS} in a-IGZO after annealing at 400 °C is ~ 10^{17} cm^{-3} and increases to ~ 10^{19} cm^{-3} as the annealing temperature increases to 450 °C. The exact value of N_{DS} in a-IGZO after annealing at 300 °C could not be estimated because the estimated value of N_D is the summation of N_{DS} and the V_O concentration in the electron-trap state. Nevertheless, we suggest that the N_{DS} increases as the annealing temperature increases because of SR. The SR-driven doping effect is weakly affected by the annealing time and strongly affected by the annealing temperature. Because SR causes a reduction in the free volume in amorphous materials,[9–11] we conclude that the microscopic origin of the SR-driven doping effect is related to increases in the concentration of V_O s located in dense networks, and V_O s in the deep-donor or electron-trap states changed to the shallow-donor state. From the kinetics perspective, the atomic mobility (that is, inverse of viscosity) in amorphous materials increases with increasing annealing temperature, which follows an Arrhenius relationship.[9] In this regard, at higher annealing temperatures, a greater reduction in free volume is expected in the limited time, as illustrated in Figure 1a. Therefore, the thin films of a-IGZO increase in density as the annealing temperatures increases because of SR, as shown in Supplementary Figure S3c.

The saturation behavior of the SR-driven doping effect indicates that the reduction in free volume is strongly determined by the annealing temperature rather than the annealing time. The free volume reduction likely occurs in a manner similar to the densification kinetics of porous amorphous films,[41] in which most of the densification is completed during the early stage of the annealing process with a sharp decrease in the densification rate as a function of annealing time. Similarly, the degree of film densification is determined by the annealing temperature rather than the annealing time. The atomic mobility of amorphous materials is related to the size of the free volume as well as to the thermal energy, and the mobility decreases with decreases in the free volume.[9,14] Thus the weak annealing time dependence of SR-driven doping suggests that the atomic mobility in a-IGZO further decreases during SR and that the rate of reduction in the free volume becomes negligible.

These SR results may provide a key to determining the origin of changes in the conduction mechanism, that is, from thermionic emission to Ohmic and P-F conduction at low and high fields, respectively. Ideally, as n_e increases to the order of 10^{17} cm^{-3}, thermionic emission should be the predominant conduction mechanism.[29] At 400 °C, although n_e in a-IGZO was nearly constant with increasing annealing time, a transition in the conduction mechanism was observed. We believe that significantly more SR is expected at the interfaces (between a-IGZO and the W electrode) than in the bulk a-IGZO because atomic mobility at interfaces is generally higher than that in the bulk.[25] Likewise, the crystallization of a-IGZO occurs at the interface under lower temperatures than in the bulk a-IGZO.[11] This phenomenon may result in sufficiently high n_e at the

interface, which in turn leads to a negligible Schottky barrier, thereby facilitating electrical conduction. We conducted the same experiments on devices composed of 40-nm-thick a-IGZO thin-film patches (Supplementary Figures S16–S19). Although the initial characteristics of the I–V curves are different, the tendencies of the changes in the conduction mechanism and N_{DS} with respect to the postfabrication annealing conditions are similar to those in the devices made from 160-nm-thick a-IGZO thin-film patches. Therefore, we believe that our results concerning the SR-driven doping effect represent universal characteristics of a-IGZO.

The inset in Figure 4b presents an Arrhenius plot of N_{DS}. We consider the average N_{DS} values in our experiments, except the 1-h results. Then, using Figure 4b, the activation energy (E_a) was found to be approximately 1.76 eV. However, the actual activation energy is higher than this estimated value because N_{DS} at 300 °C includes the concentration of V_O s in the electron-trap state. Because the occurrence of SR accompanies internal atomic rearrangement, ionic bonding energy in a-IGZO may be responsible for the calculated activation energy. The average bond energies in a-IGZO are reported to be 2.0, 1.7 and 1.5 eV for Ga-O, In-O and ZnO, respectively.[42] The SR-driven doping effect is expressed in terms of the atomic rearrangement in the devices and the changes in the density of states in a-IGZO; these factors are shown in Figures 4c and d, respectively. The density of states in a-IGZO in the as-deposited state was obtained from Kamiya et al. [3] and Ide et al.[43] During annealing, SR results in the densification of the a-IGZO thin-films (Figure 1e and Supplementary Figure S1c) and a decrease in the free volume in a-IGZO in association with greater V_O s in the dense network. Therefore, V_O in deep-donor or electron-trap states are transformed into shallow-donor states. In this respect, SR-driven doping can be used to tune the electrical conductivity of amorphous oxide semiconductors. The fact that the SR-driven doping effect exhibited a stronger dependence on the annealing temperature than on the annealing time may be used to optimize the resistance of electronic devices to thermal stress.

CONCLUSIONS

In summary, we demonstrate an SR-driven increase in the concentration of V_O s in the shallow-donor state in a-IGZO. From measurements of the changes in electrical conductance and analyses of the conduction mechanisms in the devices, we verified that SR drove the changes in the electronic states of V_O s from the deep-donor or electron-trap states to the shallow-donor state, and the energy level of the V_O s in the shallow-donor state was estimated to be approximately 0.1 eV. As the annealing temperature increased from 300 to 450 °C, N_{DS} in a-IGZO increases from $\sim 10^{16}$ to $\sim 10^{19}$ cm^{-3} (from $<10^{16}$ to $\sim 10^{18}$ cm^{-3} for n_e). These results suggest smaller free volume defects in a-IGZO exposed to higher annealing temperatures, as well as more V_O s in dense networks and consequently higher N_{DS} values. The activation energy of N_{DS} formation (approximately 1.76 eV) can be attributed to the ionic bonding of a-IGZO. SR-driven doping may offer new possibilities for controlling n_e in amorphous oxide semiconductors in addition to redox control. The strong dependence of SR-driven doping on the annealing temperature, rather than the annealing time, will have a critical role in achieving reliable thermal stress resistance in electronic devices. In future work, we hope to investigate the effects of the initial V_O concentrations (that is, the degree of oxygen non-stoichiometry) on the SR-driven concentration increases in V_O in the shallow-donor states.

CONFLICT OF INTEREST

The authors declare no conflict of interest.

1 Nomura, K., Ohta, H., Takagi, A., Kamiya, T., Hirano, M. & Hosono, H. Room-temperature fabrication of transparent thin-film transistors using amorphous oxide semiconductors. Nature 432, 488 (2004).
2 Cherenack, K. H., Münzenrieder, N. S. & Tröster, G. Impact of mechanical bending on ZnO and IGZO thin-film transistors. IEEE Electron Device Lett. 31, 1254 (2010).
3 Kamiya, T., Nomura, K. & Hosono, H. Present status of amorphous In-Ga-Zn-O thin-film transistors. Sci. Technol. Adv. Mater. 11, 044305 (2010).
4 Kamiya, T. & Hosono, H. Material characteristics and applications of transparent amorphous oxide semiconductors. NPG Asia Mater. 2, 15 (2010).
5 Zhou, N., Buchholz, D. B., Zhu, G., Yu, X., Lin, H., Facchetti, A., Marks, T.J. & Chang, R.P. Ultraflexible polymer solar cells using amorphous zinc-indium-tin oxide transparent electrodes. Adv. Mater. 19, 1098 (2014).
6 Kamiya, T., Nomura, K., Hirano, M. & Hosono, H. Electronic structure of oxygen deficient amorphous oxide semiconductor a-InGaZnO4-x: optical analyses and first-principle calculations. Phys. Status Solidi C 5, 3098 (2008).
7 Nagarajan, L., De Souza, R. A., Samuelis, D., Valov, I., Börger, A., Janek, J., Becker, K.D., Schmidt, P.C. & Martin, M. A chemically driven insulator-metal transition in non-stoichiometric and amorphous gallium oxide. Nat. Mater. 7, 391 (2008).
8 Noh, H.-K., Chang, K. J., Ryu, B. & Lee, W.-J. Electronic structure of oxygen-vacancy defects in amorphous In-Ga-Zn-O semiconductors. Phys. Rev. B 84, 115205 (2011).
9 Taub, A. I. & Spaepen, F. The kinetics of structural relaxation of a metallic glass. Acta Metall. 28, 1781 (1980).
10 Elliott, S. R. Physics of Amorphous Materials (John Wiley & Sons, Inc., New York, NY, USA, 1990).
11 Ide, K., Nomura, K., Hiramatsu, H., Kamiya, T. & Hosono, H. Structural relaxation in amorphous oxide semiconductor, a-In-Ga-Zn-O. J. Appl. Phys. 111, 073513 (2012).
12 Hosono, H. Ionic amorphous oxide semiconductors: material design, carrier transport, and device application. J. Non-Cryst. Solids 352, 851 (2006).
13 Barquinha, P., Pereira, L., Gonçalves, G., Martins, R. & Fortunato, E. Toward high-performance amorphous GIZO TFTs. J. Electrochem. Soc. 156, H161 (2009).
14 Torquato, S. Hard knock for thermodynamics. Nature 405, 521 (2000).
15 Hosono, H., Nomura, K., Ogo, Y., Uruga, T. & Kamiya, T. Factors controlling electron transport properties in transparent amorphous oxide semiconductors. J. Non-Cryst. Solids 354, 2796 (2008).
16 Kimura, M., Nakanishi, T., Nomura, K., Kamiya, T. & Hosono, H. Trap densities in amorphous-InGaZnO4 thin-film transistors. Appl. Phys. Lett. 92, 133512 (2008).
17 Nomura, K., Kamiya, T., Hirano, M. & Hosono, H. Origins of threshold voltage shifts in room-temperature deposited and annealed a-In-Ga-Zn-O thin-film transistors. Appl. Phys. Lett. 95, 013502 (2009).
18 Fuh, C.-S., Sze, S. M., Liu, P.-T., Teng, L.-F. & Chou, Y.-T. Role of environmental and annealing conditions on the passivation-free In-Ga-Zn-O TFT. Thin Solid Films 520, 1489 (2011).
19 Kim, H., Kim, K.-K., Lee, S.-N., Ryou, J.-H. & Dupuis, R. D. Low resistance Ti/Au contacts to amorphous gallium indium zinc oxides. Appl. Phys. Lett. 98, 112107 (2011).
20 Nomura, K., Kamiya, T., Yanagi, H., Ikenaga, E., Yang, K., Kobayashi, K., Hirano, M. & Hosono, H. Subgap states in transparent amorphous oxide semiconductor, In-Ga-Zn-O, observed by bulk sensitive x-ray photoelectron spectroscopy. Appl. Phys. Lett. 92, 202117 (2008).
21 Kamiya, T., Nomura, K. & Hosono, H. Origins of high mobility and low operation voltage of amorphous oxide TFTs: electronic structure, electron transport, defects and doping. IEEE J. Disp. Technol. 5, 273 (2009).
22 Kamiya, T. & Hosono, H. Roles of hydrogen in amorphous oxide semiconductor. ECS Trans. 54, 103 (2013).
23 Nomura, K., Kamiya, T., Ohta, H., Uruga, T., Hirano, M. & Hosono, H. Local coordination structure and electronic structure of the large electron mobility amorphous oxide semiconductor In-Ga-Zn-O: experiment and ab initio calculations. Phys. Rev. B 75, 035212 (2007).
24 Barin, I., Knacke, O. & Kubaschewski, O. Thermochemical Properties of Inorganic Substances (Springer, Berlin, Germany, 1973).
25 Porter, D. A. & Easterling, K. E. Phase Transformation in Metals and Alloys (Chapman & Hall, London, UK, 1992).
26 Fehlner, F. P. Low-Temperature Oxidation: The Role of Vitreous Oxides (John Wiley & Sons, Inc., New York, NY, USA, 1986).
27 Fung, T. C., Chuang, C.-S., Chen, C., Abe, K., Cottle, R., Townsend, M., Kumomi, H. & Kanicki, J. Two-dimensional numerical simulation of radio frequency sputter amorphous In-Ga-Zn-O thin-film transistors. J. Appl. Phys. 106, 084511 (2009).
28 Michaelson, H. B. The work function of the elements and its periodicity. J. Appl. Phys. 48, 4729 (1977).
29 Brillson, L. J. & Lu, Y. ZnO Schottky barriers and Ohmic contacts. J. Appl. Phys. 109, 121301 (2011).

30 Pierret, R. F. *Semiconductor Device Fundamentals* (Addison-Wesley, New York, NY, USA, 1996).

31 Shibuya, K., Dittmann, R., Mi, S. & Waser, R. Impact of defect distribution on resistive switching characteristics of Sr_2TiO_4 thin films. *Adv. Mater.* **22**, 411 (2010).

32 Padovani, F. A. & Stratton, R. Field and thermionic-field emission in Schottky barriers. *Solid-State Electron* **9**, 695 (1966).

33 Sze, S. M. *Physics of Semiconductor Devices* (John Willey & Sons, Inc., New York, NY, USA, 1981).

34 Schroder, D. K. *Semiconductor Material and Device Characterization* (John Wiley & Sons, Inc., Hoboken, NJ, USA, 2006).

35 Yeargan, J. R. & Taylor, H. L. The Poole-Frenkel effect with compensation present. *J. Appl. Phys.* **39**, 5600 (1968).

36 Connell, G. A. N., Camphausen, D. L. & Paul, W. Theory of Poole-Frenkel conduction in low-mobility semiconductors. *Philos. Mag.* **26**, 541 (1972).

37 Angle, R. L. & Talley, H. E. Electrical and charge storage characteristics of the tantalum oxide-silicon dioxide device. *IEEE Trans. Electron Devices* **ED-25**, 1277 (1978).

38 Chung, H.-J., Jeong, J. H., Ahn, T. K., Lee, H. J., Kim, M., Jun, K., Park, J.-S., Jeong, J. K., Mo, Y.-G. & Kim, H. D. Bulk-limited current conduction in amorphous InGaZnO thin films. *Electrochem. Solid State Lett.* **11**, H51 (2008).

39 Kamiya, T., Nomura, K. & Hosono, H. Electronic structures above mobility edges in crystalline and amorphous In-Ga-Zn-O: percolation conduction examined by analytical model. *IEEE J. Disp. Technol.* **5**, 462 (2009).

40 Meyer, B. K., Volm, D., Graber, A., Alt, H. C., Detchprohma, T., Amano, A. & Akasaki, I. Shallow donors in GaN—the binding energy and the electron effective mass. *Solid State Commun.* **95**, 597 (1995).

41 Bang, J. & Lu, G.-Q. Densification kinetics of glass films constrained on rigid substrates. *J. Mater. Res.* **10**, 1321 (1995).

42 Kamiya, T., Nomura, K. & Hosono, H. Supgap states, doping and defect formation energies in amorphous oxide semiconductor $a\text{-}InGaZnO_4$ studied by density functional theory. *Phys. Status Solidi A* **207**, 1698 (2010).

43 Ide, K., Kikucih, Y., Nomura, K., Kimura, M., Kamiya, T. & Hosono, H. Effects of excess oxygen on operation characteristics of amorphous In-Ga-Zn-O thin-film transistors. *Appl. Phys. Lett.* **99**, 093507 (2011).